

UC Berkeley

UC Berkeley Previously Published Works

Title

The pumice raft-forming 2012 Havre submarine eruption was effusive

Permalink

<https://escholarship.org/uc/item/7q67c11c>

Authors

Manga, Michael
Fauria, Kristen E
Lin, Christina
[et al.](#)

Publication Date

2018-05-01

DOI

10.1016/j.epsl.2018.02.025

Peer reviewed

The pumice raft-forming 2012 Havre submarine eruption was effusive

Author links open overlay panel [Michael Manga^a](#) [Kristen E. Fauria^{a,c}](#) [Christina Lin^a](#) [Samuel J. Mitchell^b](#) [Meghan Jones^c](#) [Chris E. Conway^a](#) [Wim Degruyter^a](#) [Behnaz Hosseini^a](#) [Rebecca Carey^a](#) [Ryan Cahalan^a](#) [Bruce F. Houghton^b](#) [James D. L. White^b](#) [Martin Jutzeler^c](#) [S. Adam Soule^c](#) [Kenichiro Tani^d](#)

Show more

<https://doi.org/10.1016/j.epsl.2018.02.025> [Get rights and content](#)

Highlights

-

Havre magma entered the ocean before fragmenting.

-

Clasts were produced by quenching buoyant magma in the ocean.

-

Buoyant >1 m diameter pumice blocks floated to the ocean surface.

-

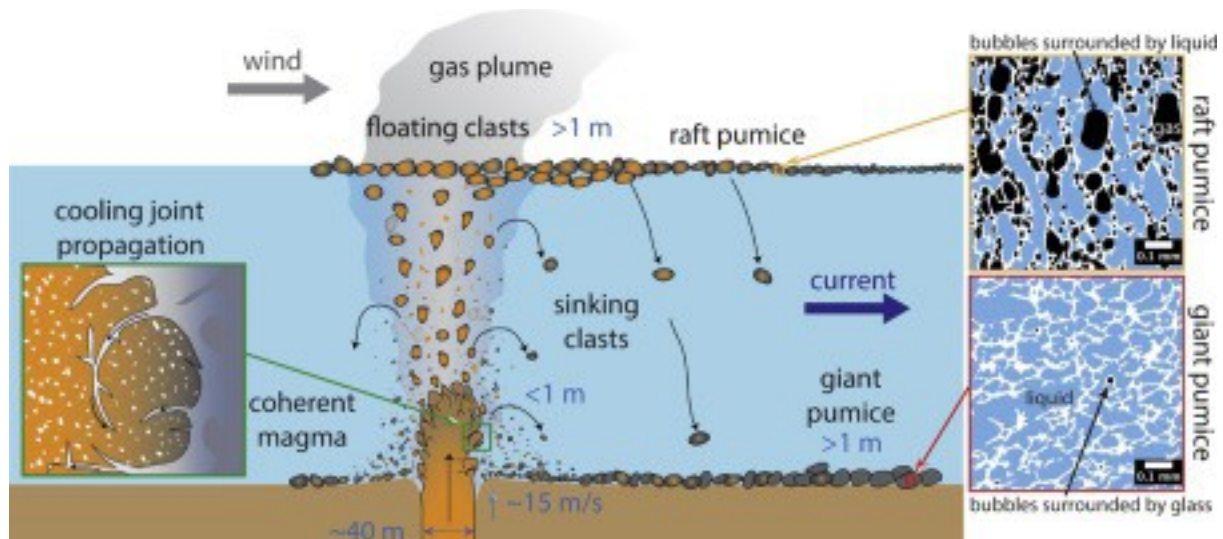
Clasts with enough isolated porosity and trapped gas floated in a raft while the rest sank.

Abstract

A long-standing conceptual model for deep submarine eruptions is that high [hydrostatic pressure](#) hinders degassing and acceleration, and suppresses [magma](#) fragmentation. The 2012 submarine [rhyolite](#) eruption of Havre volcano in the Kermadec arc provided constraints on critical parameters to quantitatively test these concepts. This eruption produced a >1 km³ raft of floating [pumice](#) and a 0.1 km³ field of giant (>1 m) pumice [clasts](#) distributed down-current from the vent. We address the mechanism of creating these clasts using a model for magma ascent in a conduit. We use water ingestion experiments to address why some clasts float and others sink. We show that at the eruption depth of 900 m, the melt retained enough dissolved water, and hence had a low enough viscosity, that [strain-rates](#) were too low to cause brittle fragmentation in the conduit, despite mass discharge rates similar to [Plinian eruptions](#) on land. There was still, however, enough exsolved vapor at the vent depth to make the magma

buoyant relative to seawater. Buoyant magma was thus extruded into the ocean where it rose, quenched, and fragmented to produce clasts up to several meters in diameter. We show that these large clasts would have floated to the [sea surface](#) within minutes, where air could enter [pore space](#), and the fate of clasts is then controlled by the ability to trap gas within their pore space. We show that clasts from the raft retain enough gas to remain afloat whereas fragments from giant pumice collected from the seafloor ingest more water and sink. The pumice raft and the giant pumice seafloor deposit were thus produced during a clast-generating effusive submarine eruption, where fragmentation occurred above the vent, and the subsequent fate of clasts was controlled by their ability to ingest water.

Graphical abstract



1. [Download high-res image \(171KB\)](#)

2. [Download full-size image](#)

- [Previous article in issue](#)
- [Next article in issue](#)

Keywords

submarine eruption

pumice

fragmentation

raft

conduit flow

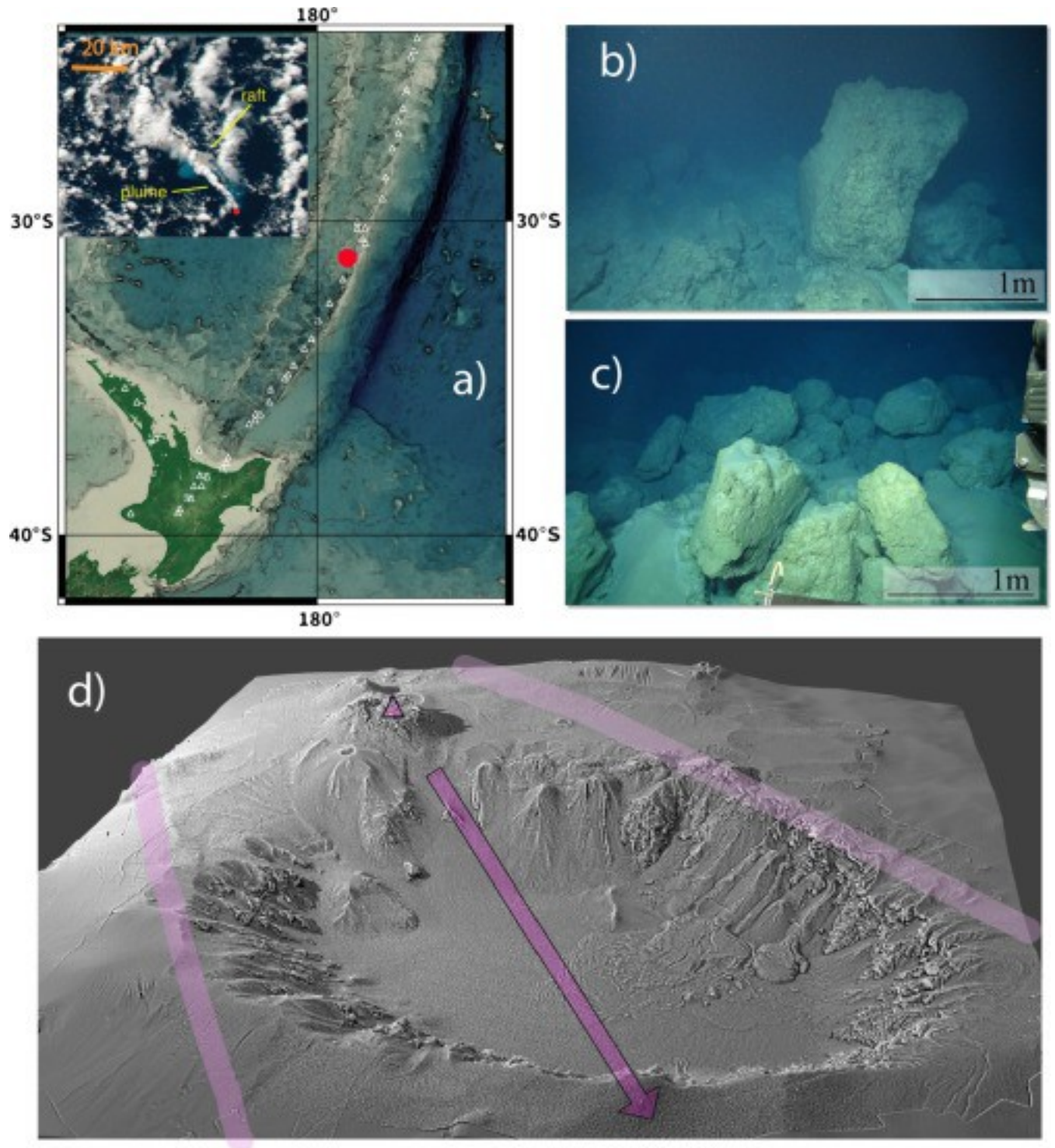
X-ray tomography

1. Introduction

Submarine volcanic eruptions may be fundamentally different from those on land owing to the high [hydrostatic pressure](#) provided by the ocean, which inhibits degassing and hence [magma](#) acceleration and fragmentation. The records of such eruptions are few and our understanding is limited by the challenge in directly witnessing eruption processes and sampling and characterizing the deposits from those eruptions. Indeed, overcoming this biased understanding of volcanic eruptions was highlighted by a National Academies report ([National Academies, 2017](#)): “What processes govern the occurrence and dynamics of submarine explosive eruptions”?

Silicic magmas that erupt more than a few hundred meters below sea-level give rise to eruption styles distinct from those on land owing to the contrasting properties of the ambient fluid (water vs air) into which the magmas erupt ([Cashman and Fiske, 1991](#)). For example, [clasts](#) that erupt at the seafloor are initially buoyant, but ingest water into [pore space](#) as they cool (e.g., [Whitham and Sparks, 1986](#)); hence fragmented magma can either rise to the surface to form rafts, or feed submarine density currents if the clasts become waterlogged ([Allen and McPhie, 2009](#)).

One distinctive [facies](#) of both modern and ancient clastic deposits from submarine silicic eruptions is voluminous deposits of giant (>1 m) [pumice](#) clasts (e.g., [Kato, 1987](#); [Kano et al., 1996](#), [Kano, 2003](#), [Allen and McPhie, 2009](#), [Allen et al., 2010](#), [Jutzeler et al., 2014](#)). These clasts often have one or more quenched margins with curvilinear joints perpendicular to the [cooling surface](#) that suggest they quenched in water (e.g., [Wilson and Walker, 1985](#), [Allen et al., 2010](#), [von Lichten et al., 2016](#); [Fig. 1](#)). Otherwise, submarine pumice vesicularities are similar to those produced in subaerial [Plinian eruptions](#) (e.g., [Barker et al., 2012](#)) and hence it has been proposed that fragmentation mechanisms are also similar for large (>1 km³) submarine equivalents (e.g., [Allen and McPhie, 2009](#), [Shea et al., 2013](#)). There are, however, textural differences: pumice clasts from deep submarine eruptions tend to have smaller bubble number densities, lack very small vesicles (<10 μm), and display a narrower range of modal vesicle sizes ([Rotella et al., 2015](#)). Clasts have also been proposed to form from buoyant bubbly magma as it exits the vent by “viscous detachment or by the development of cooling joints” ([Rotella et al., 2013](#)), an eruption style that would not fit neatly into either the “effusive” or “explosive” categories used to describe subaerial eruptions. Pumice clasts can also form by [spallation](#) from a pumiceous carapace on effusive domes (e.g., [Cas and Wright, 1987](#), [Kano, 2003](#), [Allen et al., 2010](#)).



1. [Download high-res image \(560KB\)](#)
2. [Download full-size image](#)

Fig. 1. (a) Location of the Havre volcano (red circle) in the Kermadec arc. Inset shows the raft and plume on 19 July, 01:26 UTC. Inset scale bar is 20 km long. Plume and raft show the transport direction to the northwest. Example seafloor

giant [pumice clasts](#) showing curvilinear surfaces (b) and typical deposit (c). (d) Shaded relief map showing the vent location (triangle) at a depth of 900 m; arrow shows the dispersal axis of seafloor giant pumice (the same as the transport direction in a), and the light purple lines bound the region containing those clasts. Caldera is 4.5 by 5 km in size. Viewing direction is looking south. (For interpretation of the colors in the figure(s), the reader is referred to the web version of this article.)

In July 2012, approximately 1.2 km³ of [rhyolite](#) pumice clasts erupted at a water depth of 900 m from the submarine Havre volcano in the Kermadec [volcanic arc](#) ([Carey et al., 2014](#); [Fig. 1](#)). The majority of the pumiceous material formed a raft of floating clasts that was widely dispersed in the western Pacific Ocean ([Jutzeler et al., 2014](#), [Carey et al., 2018](#)). A second clastic product of this eruption is a 0.1 km³ deposit of giant pumice clasts on the seafloor around the inferred vent. An outstanding question is whether these seafloor giant pumice clasts and raft pumice originated from the same eruptive phase. Though not conclusive, the vesicularities, composition, microtextures (e.g., bubble number densities, [crystallinity](#), microlite mineralogy), and macrotextures (e.g., banding), are similar as is their primary axis of dispersal ([Carey et al., 2018](#)). If the raft and seafloor pumice did originate from the same eruptive episode, their different fate, i.e., whether they floated or sank, thus requires seafloor giant pumice to ingest water more effectively than clasts that were transported into the raft.

Here we use a model for magma ascent, constrained by estimates of the eruption rate for the pumice raft and a variety of measurements on erupted materials, to show that buoyant magma reached the seafloor prior to fragmenting. We then investigate how pumice clasts from the raft and seafloor ingest water as they cool and find that seafloor pumice ingest water more efficiently by trapping very little gas. We thus infer that vesicular coherent magma extruded into the ocean. The magma quenched and fragmented non-explosively to form the pumice clasts that then either remained afloat because they retained enough gas or, if they waterlogged, settled to the seafloor.

2. Methods

2.1. Conduit model

[Magma](#) ascent is simulated using a one-dimensional two-phase model for [steady flow](#), modified from [Degruyter et al. \(2012\)](#) and [Kozono and Koyaguchi \(2009\)](#). Pressure at the vent is 9 MPa corresponding to a water depth of 900 m. The conduit length is 8.1 km with a pressure at its base of 200 MPa. [Crystallinity](#) is 5% ([Carey et al., 2018](#)) and [crystals](#) do not grow or nucleate during ascent. The effects of crystals and bubbles

on viscosity are based on the models of [Costa \(2005\)](#) and [Llewellyn and Manga \(2005\)](#), respectively (supplement S1). Water content in the melt is 5.8 weight % based on 16 plagioclase-hosted [melt inclusions](#) from a seafloor giant [pumice clast](#) (supplement S2). Number density of bubbles is 10^{14} m^{-3} ([Rotella et al., 2015](#)), high enough that we can assume equilibrium bubble growth ([Gonnermann and Manga, 2005](#)); we obtain similar ascent rates for number densities 100 times lower and higher. The effects of temperature and dissolved water on viscosity are computed using [Giordano et al. \(2008\)](#) and the measured composition (supplement S3) and water content. Temperature is set to $850 \pm 20 \text{ }^\circ\text{C}$ based on cpx-opx Fe–Mg exchange ([Putirka, 2008](#)) in ten measured cpx and opx compositions. Magma can fragment in the conduit if the [strain-rate](#) $\dot{\gamma}$ exceeds a critical value (e.g., [Papale, 1999](#))

$$(1) \dot{\gamma} > 10^{-2} G / \mu,$$

where $G = 10^{10} \text{ Pa}$ is the [shear modulus](#) (e.g., [Simmons, 1998](#)) and μ is the melt viscosity. We compute both the strain-rate at the conduit walls and the elongation strain-rate in the center of the conduit.

It is important to recognize that in addition to uncertainties in magma properties there are also model assumptions that affect strain-rates, ascent velocity, and vesicularity at the vent. For example, the ascending magma is assumed to be isothermal and Newtonian, we neglect viscous heating and shear localization in the magma, and we do not permit non-equilibrium bubble growth. We also use a geometrically idealized conduit shape. In addition, we assume that at any given depth the bubble size is uniform and use this bubble size to compute a permeability. There are, however, bubbles much larger than the mean size which, owing to the [nonlinearity](#) of permeability-bubble size relationships, could lead to higher permeability and more [outgassing](#).

2.2. Floatation experiments

To determine the propensity for Havre pumice clasts to remain afloat after reaching the raft at the [ocean surface](#), we conducted 11 experiments in which we measured the amount of liquid water and trapped gas within cm-sized clasts from the Havre raft (7 samples) and fragments of seafloor giant pumice (4 samples). We heated dry raft clasts and giant pumice fragments to a range of temperatures up to $700 \text{ }^\circ\text{C}$ and placed them on the water surface for ten minutes. We then rapidly encased the clasts in wax – to minimize further changes in the distribution of internal fluids – and imaged the clasts at $1.22 \text{ } \mu\text{m}$ resolution using [X-ray](#) computed microtomography (XRT) with 30 keV monochromatic X-rays. To enhance the absorption contrast between the water and glass, we used a 13 weight % [potassium iodide](#) solution. Additional imaging details are

provided in supplement S4. From the XRT images, we identified the volumetric content of glass, liquid water, and trapped gas within the clasts using [machine learning](#) algorithms to segment these three phases ([Fauria et al., 2017](#)).

To further quantify pumice floatation dynamics, we measured the floatation time of room temperature raft and seafloor clasts. To measure floatation times, we placed dry and [ambient temperature](#) clasts in water and noted the time at which they sank. Before the experiments, we cleaned the clasts in an ultrasonicator for ~10 min and then dried them. Once the experiments were initiated, we monitored the clasts with a camera and noted the time at which the clasts sank to the nearest minute. If clasts continued to float after the first six months of the experiments, we stopped monitoring with a camera and began checking on the clasts approximately daily and then weekly once the experiments progressed past the first year.

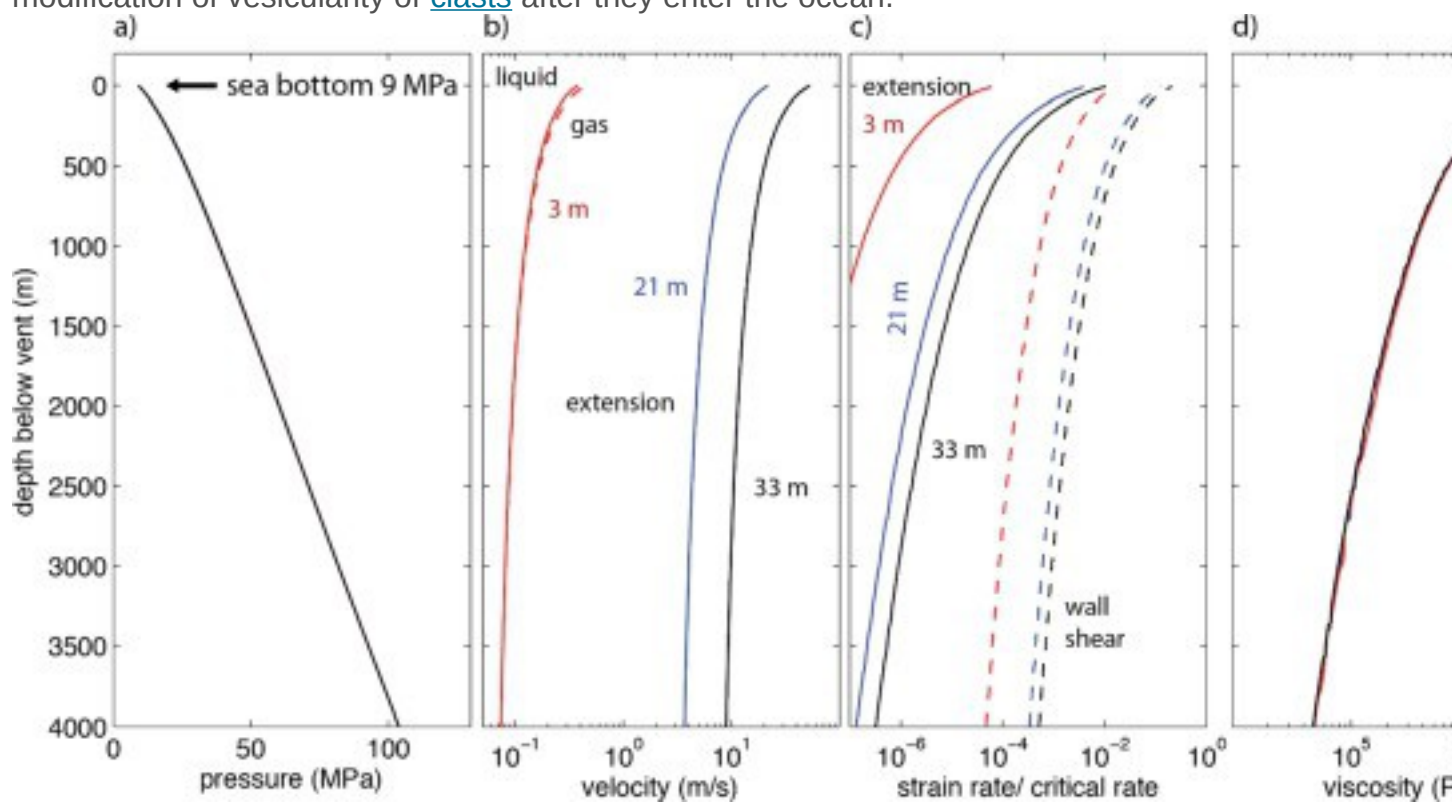
We measured clast weight before and after the experiments. For a subset of the clasts, primarily the seafloor clasts, we measured clast volume using [photogrammetry](#). Specifically, we took 100–180 photographs per clast using a Canon DSLR camera with an extension tube. We processed the images and constructed volume models (Poisson surface reconstructions) using VisualSFM and MeshLab softwares. In cases where the clasts were too small to accurately measure volume using photogrammetry, we estimate pumice volume using pumice mass assuming a clast [porosity](#) of 83% ([Carey et al., 2018](#)).

2.3. Isolated porosity

Differences in isolated porosity between the raft and seafloor samples are unresolvable in the XRT scans. We thus use [helium](#) pycnometry to quantify the connected and unconnected [pore space](#). Samples were cored, washed, dried, and weighed. The volume of the cylindrical cores was calculated based on the mean of 10 measurements of the sample diameter and height. The volumes of the solid phase and isolated porosity were measured using a He-pycnometer at the University of Oregon using methods described in [Giachetti et al. \(2010\)](#). The pycnometry measurements and bulk volume were used to calculate the connected porosity. One seafloor sample and one raft sample were crushed, weighed, and analyzed using He-pycnometry in order to determine the solid density. The bulk vesicularity was calculated from the solid [density](#), [bulk](#) volume, and bulk density. The isolated vesicularity was calculated from the difference between the bulk vesicularity and connected vesicularity.

3. Results

[Fig. 2](#) shows how ascent velocity, mean bubble size, melt viscosity, and vesicularity vary with depth in the conduit for conduit radii of 3, 21 and 33 m. The corresponding mass eruption rates are 4.2×10^3 , 1.0×10^7 and 6.2×10^7 kg/s, respectively. This model reproduces the observed vesicularity of about 80–90% and modal vesicle size ([Rotella et al., 2015](#), [Carey et al., 2018](#)). A conduit radius of 21 m leads to a mass eruption rate similar to the time-averaged value inferred from the volume of the [pumice](#) raft and the estimated duration of the raft-forming stage of the eruption, 9×10^6 kg/s ([Carey et al., 2018](#)). For this eruption rate, [Fig. 2b](#) shows that the gas and melt remain coupled and there is negligible [outgassing](#) during ascent. The model does not account for any further modification of vesicularity of [clasts](#) after they enter the ocean.



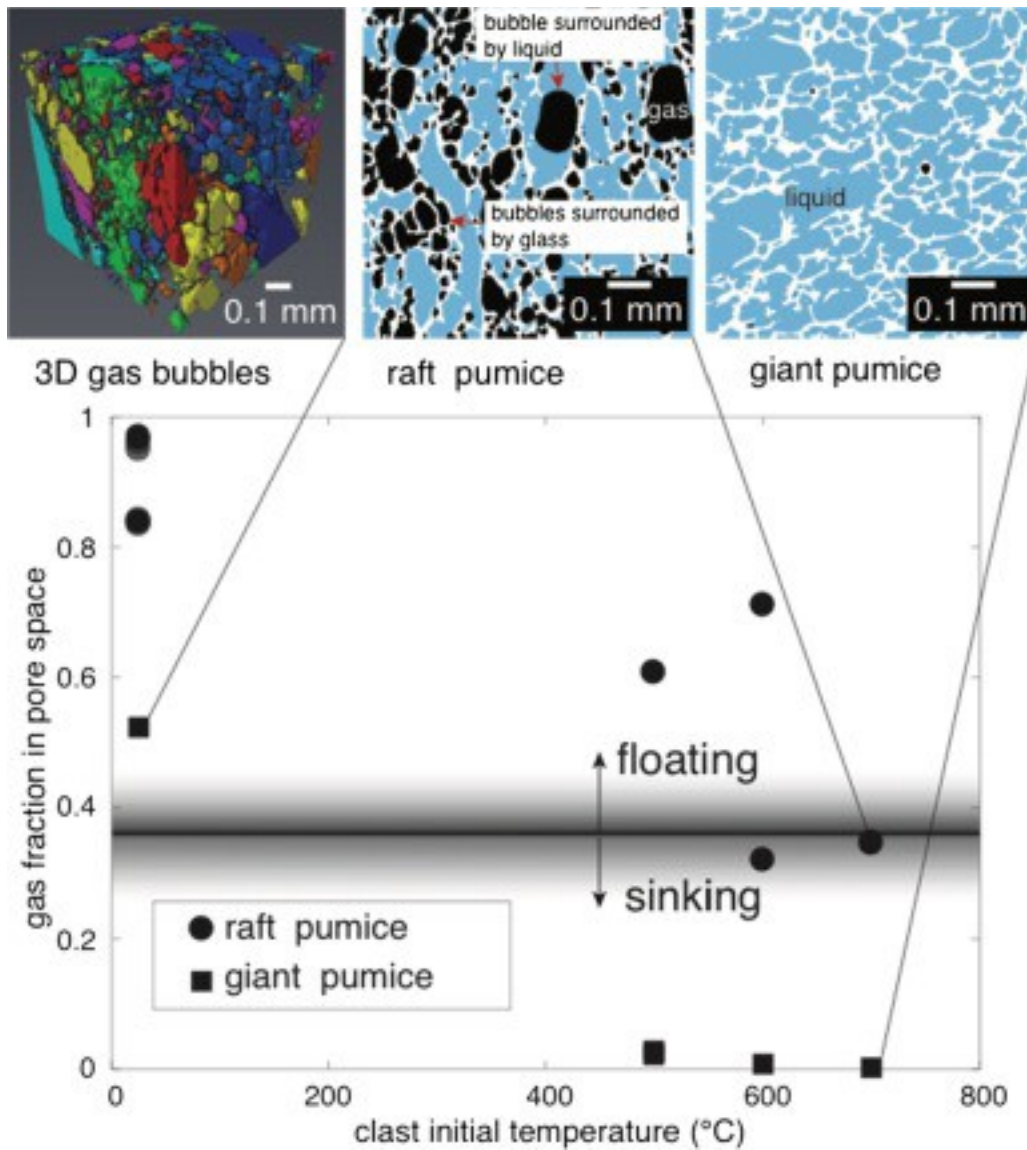
1. [Download high-res image \(163KB\)](#)
2. [Download full-size image](#)

Fig. 2. [Magma](#) ascent and gas escape, computed using the steady one-dimensional model of [Degruyter et al. \(2012\)](#) with melt properties for the Havre 2012 [rhyolite](#) eruption, showing how pressure (a), melt (solid curves) and gas (dashed curves) velocities (b), [strain-rate](#) relative to that needed to cause brittle fragmentation (c), magma viscosity (d), and vesicularity (e) varies with depth below the seafloor. Three conduit radii are assumed, 3, 21 and 33 m. Only the upper 4 km of the conduit are shown. Additional parameters: the [percolation](#) threshold for gas flow through the magma

is zero, [tortuosity](#) factor is 3, bubble throat to radius ratio is 0.31, and the [friction coefficient](#) for gas flow through the magma is 10 (supplement S1 for details).

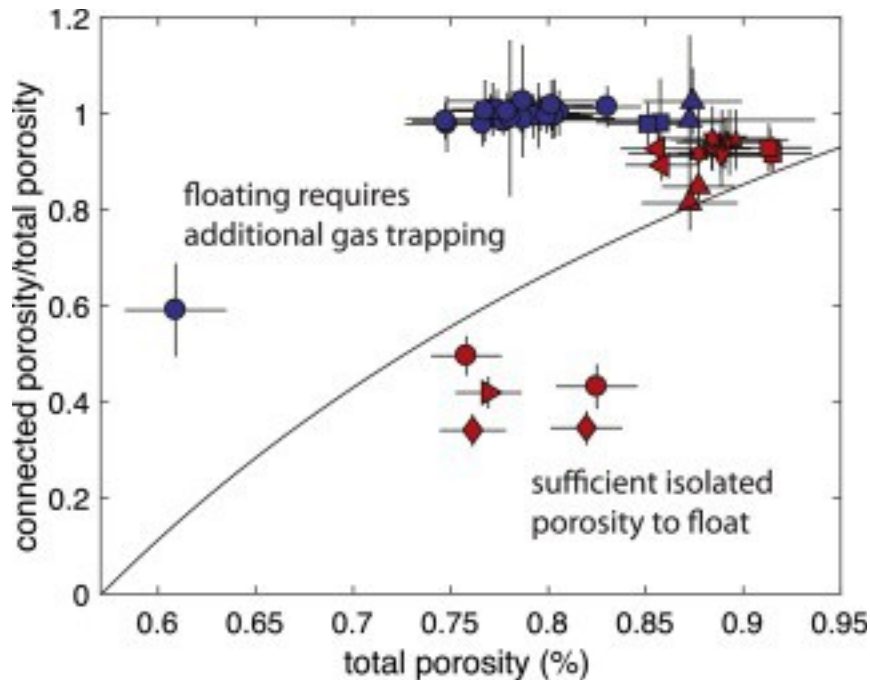
There are uncertainties in all model parameters including, critically, those that affect viscosity: water content and temperature. However, the main conclusions are not sensitive to reasonable ranges in these parameters. For example, if we reduce the water content to 5% and temperature to 820 °C, even for an eruption rate an order of magnitude greater than inferred, 1×10^8 kg/s, the [strain-rate](#) is still a factor of 5 too low to cause melt to fragment based on equation (1).

[Fig. 3](#) shows that reheated (>500 °C) Havre raft pumice can retain enough gas to remain buoyant. By comparison, fragments from the seafloor giant pumice are almost fully saturated (<0.05 [volume fraction](#) gas) after they are reheated above 500 °C and placed on the water surface. The results from these experiments demonstrate that hot Havre seafloor giant pumice draw in considerably more water than raft pumice. In raft pumice, some of the gas is trapped by the infiltrating water (red arrow), but there is also a significant amount of unconnected [porosity](#) (isolated bubbles). This difference is further highlighted by the pycnometry measurements. [Fig. 4](#) shows the connected and unconnected porosity analysis and reveals that seafloor giant pumice has fully connected porosity whereas raft pumice always contains isolated bubbles. These differences may be documenting samples from different parts of the conduit, or samples that experienced different and continued vesiculation histories in the water column. A thorough analysis of textures from raft and seafloor samples may reveal not only why some clasts float, but provide further insights into ascent processes in the conduit and water column.



1. [Download high-res image \(190KB\)](#)
2. [Download full-size image](#)

Fig. 3. Initially hot [pumice](#) ingests more water than cold pumice, and giant pumice fragments (unknown locations within the larger clast) recovered from the seafloor ingest more water than pumice from the raft. A different pumice [clast](#) is used for each experiment and hence data point. The horizontal line shows the trapped gas fraction needed to keep a clast with a vesicularity of 80% buoyant. The two images on the upper right are 2D slices through their 3D images showing the distribution of glass (white), trapped gas (black), and liquid water (blue). Upper left shows the 3D shapes of trapped gas bubbles with a different color assigned to different gas bubbles.



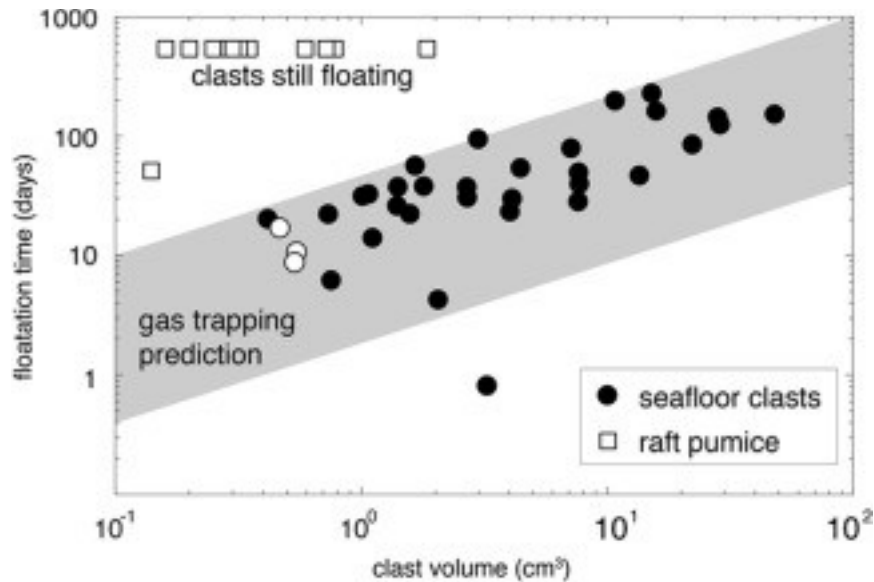
1. [Download high-res image \(152KB\)](#)
2. [Download full-size image](#)

Fig. 4. Connected fraction of total [porosity](#) vs. total porosity for seaflower giant [pumice](#) samples (blue) and raft samples (red). The measurements were conducted on multiple cores from three seaflower giant pumice samples and nine raft samples. Distinct samples are shown with different symbols. Excluding one seaflower pumice measurement, which was collected from a breadcrusted exterior, the seaflower giant pumice samples all have >99% connected porosity. All raft samples contain isolated vesicles. Shown with the curve is the amount of connected porosity needed, as a function of total porosity to allow [clasts](#) to sink if the connected [pore space](#) fills completely with water (equation [\(B.9\)](#)).

[Fig. 5](#) shows clast volume versus floatation time. We find that floatation time increases with clast size and that raft pumice float orders of magnitude longer than seaflower pumice. We compare pumice floatation times to a diffusion model for pumice floatation from [Fauria et al. \(2017\)](#). The model predicts that floatation time scales as

$$(2)\tau=4R^2Da\theta^2,$$

where τ is time, $2R$ is clast diameter, $Da=1.9\times 10^{-9}$ m²/s is air-water [diffusivity](#) ([Fauria et al., 2017](#)), and θ is the fraction of [pore space](#) containing liquid water. The shaded region in [Fig. 5](#) shows predictions of equation [\(2\)](#) with θ between 0.1 and 0.5. Seaflower clasts match the diffusion model prediction while raft pumice float much longer than predicted and, indeed, have yet to sink. The presence of isolated bubbles ([Fig. 4](#)) may explain why cold raft pumice float much longer than theoretical models predict.



1. [Download high-res image \(56KB\)](#)
2. [Download full-size image](#)

Fig. 5. [Clast](#) volume versus floatation time (the time at which clasts sink). Data points above “still floating” show clasts that were still floating at the time of manuscript submission. Open data points represent clasts for which volume was calculated from weight and by assuming [porosity](#); black data points represent clasts for which volume was measured using [photogrammetry](#). From calculated porosity from mass and volume measurements we find that seafloor clasts have porosities of $85.6 \pm 3.2\%$. The grey bar represents a floatation time prediction from equation (2) and assuming $0.1 < \theta < 0.5$. The behavior of seafloor clasts matches the gas trapping prediction while that of raft clasts does not. Error bars are smaller than the data points.

4. Discussion

We now address, in order, three basic questions about the 2012 Havre eruption. Where and why did the [magma](#) fragment? What processes form meter-sized [clasts](#)? Why do some [pumice](#) clasts float (raft pumice) and others sink (seafloor giant pumice)?

4.1. Fragmentation

From the conduit model, [strain rates](#) never become large enough to cause brittle fragmentation within the conduit of the Havre eruption. Instead, at 86% vesicularity, the erupting magma is less dense than sea water and hence will continue to rise above the vent rather than creating a dome. What processes then create the pumice? We do not favor buoyant detachment of blebs by [gravitational instabilities](#), one mechanism suggested for example by [Rotella et al. \(2013\)](#), because the separation of blebs is slow compared to the inferred [extrusion](#) velocity for the Havre eruption and we did not see

fluidal-shaped clasts either near the vent or in samples from the raft. For a bleb of length l and radius r buoyantly rising above the extruding magma, the velocity $dl/dt \approx (\rho_w - \rho_c)gr / 2\mu \ln(l/r)$, where ρ_c is clast density, ρ_w is water density, and g is gravity ([Olson and Singer, 1985](#)). This is a Stokes flow scaling, appropriate because the magma viscosity controls extrusion prior to fragmentation. Choosing $l=2r$ for equant bleb, $\mu=5 \times 10^6$ Pa s ([Fig. 2](#)), $\rho_w - \rho_c = 500$ kg m⁻³ ([Rotella et al., 2015](#), [Carey et al., 2018](#)), and $l=5$ m, we obtain an ascent speed of 4 cm/s, much less than the velocity at the vent of 14 m/s ([Fig. 2](#)). The melt is so viscous that ductile processes are too slow to produce clasts.

Instead, we suggest that the surface of extruded magma will quench in the ocean, producing a network of cracks perpendicular to the magma surface. Highly vesicular magma is prone to quench fragmentation and the temperature difference between magma and seawater is sufficient to create cracks ([van Otterloo et al., 2015](#)), possibly aided by continued vesiculation. [Crack propagation](#) speeds can be tens to hundreds of meters per second ([van Otterloo et al., 2015](#)) so that a large volume of fragmented debris can be produced very quickly. Although a range of fragment sizes will be produced, they will not be able to separate and rise unless they can also float upwards fast enough from the extruding magma. Smaller fragments may weld together, or may break off larger clasts or the side of the extruding spine of magma if spine extends above the vent.

4.2. Separating pumice from extruding magma

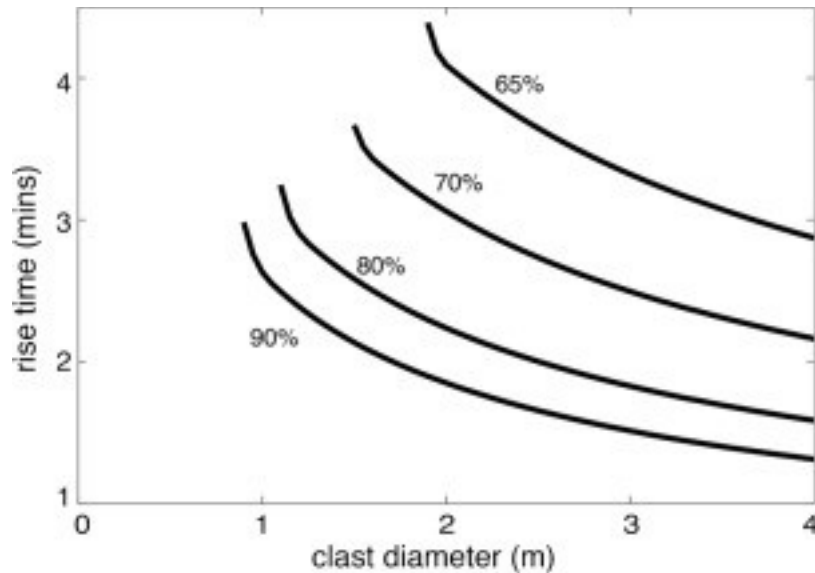
The terminal rise speed U of clasts produced by quenching and surrounded by water, idealized here as spherical with radius R , is

$$(3) U = 8(\rho_w - \rho_c)gR^3 / 3\mu C_D$$

Given the very high Reynolds number ($\sim 10^7$), the drag coefficient C_D is approximately 0.3 (e.g., [Batchelor, 1967](#)). Equation (2) also neglects [entrainment](#) by the buoyant warm water heated by the clasts, which would increase velocity. With a conduit radius of 21 m the vent velocity is 14 m/s ([Fig. 2](#)), and clasts with $R > 4.5$ m will rise faster than the extrusion speed, at least before they ingest water. Exit velocity is inversely related to conduit radius owing to mass conservation. If the vent widens by 40% at the seafloor, the minimum radius R for detachment decreases to 1.2 m. There are uncertainties in both the mass eruption rate that constrains the exit velocity and the parameters that affect the minimum size of clasts computed from equation (3), but predicted meter-sized clasts are similar to typical sizes of the giant pumice on the seafloor, averaging 1–1.6 m near the vent and increasing with dispersal distance ([Carey et al., 2018](#)).

4.3. Reaching the sea surface

Clasts that detach from the extruded magma will rise through the ocean until they saturate with water. Once saturated, clasts will become negatively buoyant and sink to the seafloor. For meter-sized clasts, water ingestion is limited not by permeability but by the ability of water vapor in the clast to cool, condense and draw in liquid (appendix [A](#)). As cooling is slower than permeable flow, the rate of heat loss from the interior of the pumice will determine the time to saturation. To compute the evolution of clast density through water ingestion, and hence their ascent through the ocean, we model the cooling, condensation, and thus flow of liquid water into spherically symmetric clasts using experimentally measured rates of heat loss, and compute the rise speed of the clasts using equation [\(3\)](#) from the time-evolving mean clast density (assuming fully connected porosity). We allow gas in the clasts to expand as the ambient pressure decreases (appendix [B](#)), which is significant because water vapor density is $>15 \text{ kg/m}^3$ at 900 m water depth and $\sim 1 \text{ kg/m}^3$ at the surface. Additional joints within clasts would enhance water ingestion and cooling beyond what we model. We neglect any possible further vesiculation within clasts as they rise through the ocean. Although clasts may remain hot as they ascend and can continue to exsolve water, vesicles need not grow if the [pore space](#) is connected to permit gas leakage to the ocean (e.g., [Kueppers et al., 2012](#)). [Fig. 6](#) shows the time required for clasts of different vesicularities to reach the [ocean surface](#) before they become negatively buoyant in water. Meter-sized clasts, such as the seafloor giant pumice, are expected to reach the raft at the ocean surface and will have ingested little water. The initial sizes of raft pumice are not known, but [Fig. 6](#) suggests that a minimum size of about one meter is required for clasts to reach the surface.



1. [Download high-res image \(44KB\)](#)
2. [Download full-size image](#)

Fig. 6. Time required for [clasts](#) to reach the [ocean surface](#) from a depth of 900 m as a function of their size and vesicularity (assumed constant during ascent). Clasts with diameters smaller than those for which the curves begin (to the left of the curves) will ingest enough water to become negatively buoyant before reaching the surface. Rise speed evolves according to equation (2) and clast density is computed from the water ingestion model (appendix B).

4.4. To sink or float?

The long-term fate of floating pumice on the sea surface depends on their ability to ingest additional water as they float. The ascent model predicts that there is virtually no liquid in meter-sized and larger clasts as they reach the sea surface owing to the expansion of vapor in the clasts during ascent (appendix B). However, the seafloor deposit of giant pumice comprises clasts up to 9 m in diameter ([Carey et al., 2018](#)). Some of those may include pumices that are large enough to reach the sea surface, but are trapped underneath floating pumice and remain fully surrounded by water, in which case we would expect them to sink once the water vapor cools and condenses ([Allen et al., 2008](#)). Others must have reached the sea surface and subsequently saturated with water.

Once pumice reaches the sea surface, we expect air to replace most of the water vapor in the pore space because [gas diffusion and exchange](#) is rapid, and is further enhanced as clasts crack or break. Air-filled pumice is known to float much longer (e.g., [Whitham and Sparks, 1986](#); [Manville et al., 1998](#); [Dufek et al., 2007](#), [Jutzeler et al., 2017](#)) than

the time it takes for porous flow to allow water to infiltrate ([Vella and Huppert, 2007](#)). Instead, the ability of clasts to float is controlled by the propensity of the infiltrating water to trap gas bubbles within the pore space and/or the presence of isolated vesicles. If enough gas is trapped during infiltration of water, the clasts will float until this gas diffuses through the water and out of the clast ([Fauria et al., 2017](#)).

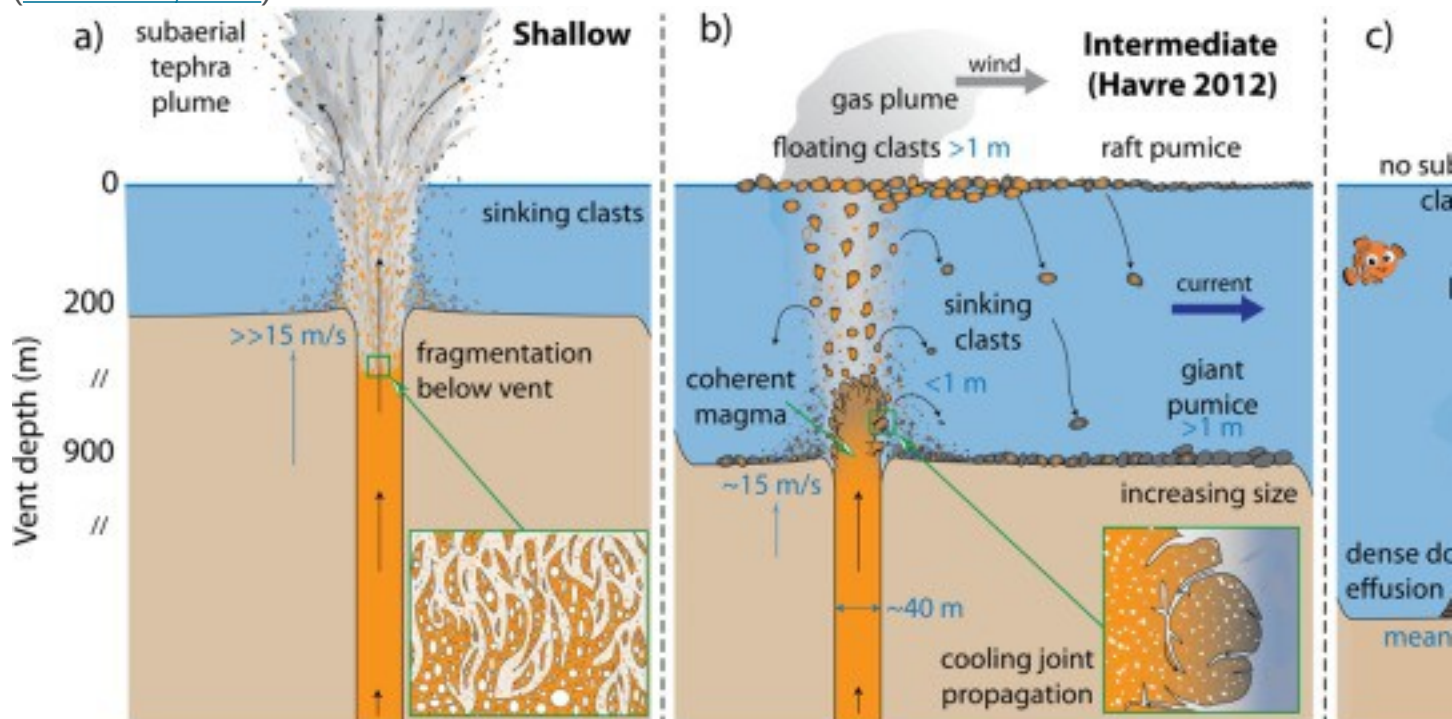
The difference in isolated and connected [porosity](#) can partially explain the propensity for raft pumice to float, however, additional gas trapping is required for most clasts ([Fig. 4](#)). Our experiments confirm that fragments of seafloor giant pumice ingest more water and trap less gas than raft pumice, and hence more rapidly become negatively buoyant. The presence of elongate "tube" vesicles in some seafloor pumice has further implications for why some clasts sink preferentially to others. The elongate structure, high connectivity and anisotropic permeability of such vesicles would permit rapid clast saturation and subsequent sinking to the seafloor ([Wright et al., 2006](#)). The diversity of these textures within pumice deserves more detailed microtextural analysis.

We thus propose that what separates pumice into the raft is their ability to trap gas and the presence of isolated vesicles; clasts that cannot retain enough gas sink. Those that trap gas and/or have sufficient isolated vesicles float. Presumably the difference in gas trapping results from differences in topology of the pore space such as the number of dead-end pores. We could not, however, identify any key differences in our images. We note several caveats. First, we are not able to do experiments on meter-sized raft or seafloor clasts owing to the lack of intact samples and our inability to measure and image the infiltration at such large scales. We thus assume that the smaller fragments we imaged are representative of the larger clasts from their respective units. Second, we do experiments on quenched samples, whereas the vesicularity and texture of the pumice may evolve during quenching and also after their initial fragmentation. Larger clasts should take longer to ingest water, explaining why seafloor pumice clast size increases with distance from the vent ([Carey et al., 2018](#)).

4.5. The effusive eruption of Havre

The raft-forming Havre eruption was not explosive in the same manner as subaerial pumice clast-forming eruptions. This submarine style of pumice-generating eruption requires an eruption depth that is not-too-deep and not-too-shallow ([Fig. 7](#)). In deeper water, with the critical depth depending on the water content of the melt, the magma will not be buoyant and will form a [lava flow or dome](#) ([Fig. 7c](#)). In shallower water, the melt viscosity will be higher owing to greater gas [exsolution](#) and the magma may undergo brittle fragmentation in the conduit ([Fig. 7a](#)). For the Havre mass eruption rate,

composition, and water content, a vent depth of 2.8 km will lead to the erupting magma being denser than seawater (1030 kg/m^3), and a vent shallower than 290 m will allow the magma to fragment in the conduit (21 m radius) assuming that the criterion given by equation (1) is accurate. It is worth noting that the Taupo eruption which also produced giant pumice fragments, and was dominated by Plinian-phreatoplinian explosions and magmatic fragmentation in the conduit, occurred in water depths that were never more than 200 m (Wilson and Walker, 1985, Houghton et al., 2003). Mass discharge rate also matters because low ascent rates enable outgassing. For example, at Havre multiple lava domes with low-to-moderate vesicularity extruded in 2012 at the same water depth as the vent that produced the giant pumice clasts. At Sumisu Dome C in the Sumisu Dome Complex, Izu Bonin Arc, Japan, silicic pumiceous dome carapaces at 1100–1300 mbsl have high vesicularity, between 60–85%, and did not produce a clastic deposit (Allen et al., 2010).



1. [Download high-res image \(256KB\)](#)
2. [Download full-size image](#)

Fig. 7. Schematic illustration of the eruption of magma with Havre composition and water content, but at different depths: (a) shallow enough that fragmentation occurs in the conduit, (b) Havre vent depth, and (c) deep or ascended slow enough that vesicularity is <58%. In (b), clast size in the raft decreases with transport owing to abrasion. Inset in each panel illustrates the manner in which clasts might form, either within the conduit (a), or quenching in water (b and c). Panel (b) illustrates the settling of

smaller clasts close to the vent, the rise of large, hot clasts to the [sea surface](#), the trapping of hot [pumice](#) beneath the sea surface, and the settling of giant pumice out of the raft due to water ingestion. The relative temperature gradient of melt to glass in clasts given from orange to grey, respectively. White shapes are vesicles. Liquid water is blue. Not to scale.

The 2012 eruption that produced the pumice raft partly conforms to the eruption style proposed by [Rotella et al. \(2013\)](#) in which bubbly magma enters the ocean and clasts detach from the extruding magma; we favor “cooling joints” and other mechanical stresses over “viscous detachment” for Havre because the effusion velocity is so high and because we lack evidence for any wholly or partly bleb-shaped clasts; ductile processes, however, may be important for creating floating clasts from less viscous magmas (e.g., [Kueppers et al., 2012](#)). As noted by others (e.g., [Cas and Giordano, 2014](#), [Allen and McPhie, 2009](#), [White et al., 2015](#)), terminology such as explosive and effusive, developed for subaerial eruptions and their deposits, may not translate well to the submarine realm where high [hydrostatic pressure](#) and the cooling effects of liquid water can modulate fragmentation.

Given that submarine giant pumice deposits are common products of historical eruptions and well documented in the rock record ([Reynolds et al., 1980](#), [Kano et al., 1996](#), [Risso et al., 2002](#), [McPhie and Allen, 2003](#), [Kano, 2003](#), [Allen and McPhie, 2009](#), [Allen et al., 2010](#), [Jutzeler et al., 2014](#), [von Lichten et al., 2016](#)), we infer that the 2012 Havre eruption may be an example of a relatively common style of deep submarine volcanic eruption. Modern intra-oceanic arcs, such as the Kermadec, Izu, Bonin, Mariana, and South Sandwich arcs contain many deep submarine silicic volcanoes, and similar eruptions may be common.

5. Conclusions

The 2012 [pumice](#) raft-forming eruption was produced from a vent that extruded buoyant vesicular [rhyolite](#) into the sea at speeds >10 m/s. This lava fragmented by quenching in the ocean to produce three [subpopulations](#) of [clasts](#). Large clasts (>1 m) rose to the [sea surface](#) without ingesting enough water to sink. Those large clasts with sufficient isolated vesicles and/or trapped gas remained afloat in the raft. Large clasts that did not retain enough gas, and those that were trapped beneath the pumice raft, sank to create the seafloor giant pumice. Smaller clasts would not have reached the surface, ingesting water quickly and settling close to the vent, or were transported by currents if small enough.

The eruption style documented at Havre may be dominant for submarine silicic eruptions, as most submarine vents are at depths greater than a few hundred meters. Voluminous deposits of giant pumice clasts are a product, and thus an indicator, of large, deep silicic effusive eruptions. This eruption style can partition most of the mass into distal and [global ocean](#) basins, which has implications for how we interpret past events and may ultimately lead to a re-evaluation of the volumes and magnitudes of submarine eruptions in the past.

Acknowledgments

MM, KF, CL and BH are supported by NSF [1447559](#). SM and BH are supported by NSF [1357443](#). RJC was funded by the Australian Research Council ([DP110102196](#), [DE150101190](#)). AS is supported by NSF [1357216](#). MJ is supported by a National Defense Science and Engineering Graduation Fellowship. [CEC](#) is supported by the Japan Society for the Promotion of Science ([JSPS P16788](#)). XRT was enabled by the Lawrence Berkeley National Lab Advanced Light source, beamline 8.3.2, and guidance from Dula Parkinson. Additional support was provided by the Marsden Fund and the 2017 Student Mentoring and Research Teams (SMART) Program, Graduate Division, University of California, Berkeley. Fumihiko Ikegami created [Fig. 1d](#). Brian Monteleone provided assistance in SIMS analysis of [melt inclusions](#) at the Northeast National [Ion Microprobe](#) Facility. Melissa Rotella provided the raft [clasts](#) used in the floatation experiments. Thomas Giachetti provided assistance with He-pycnometry. We thank Tushar Mittal, Dan Fornari, Jocelyn McPhie, Ray Cas and an anonymous reviewer for comments, and the rest of the MESH team, [ROV](#) and [AUV](#) operators, and Roger Revelle crew for making this science possible.

Author contributions

MM and WD modeled [magma](#) ascent. KF and CL performed the ingestion experiments and analysis. RC and SM measured volatiles. CC measured composition. KF and BH did the floatation experiments. MJ measured [porosity](#). KF and MM developed the [clast](#) ascent and ingestion model. All authors contributed to sample collection, interpretation and writing.

Appendix A. Why ingestion is not likely to be limited by permeability for large clasts

As the interior of vapor-filled [pumice](#) cools, vapor condenses and draws in liquid water. Whether heat loss or permeability limits this ingestion of liquid depends on the ability of a [clast](#) to lose heat compared to the ability of liquid to flow into the clast – the slowest process will govern liquid ingestion.

The condensation of vapor and heat loss from the clast is similar to the classic Stefan problem except that [advection](#) of heat by liquid water drawn into the clast may dominate the heat transport. An energy balance at the vapor–liquid interface balances the conductive transport across that interface with the [latent heat](#) released

$$(A.1) -\kappa dT/dx = \rho_s \phi L u$$

where u is the fluid velocity, L the latent heat, ρ_s is the density of steam, ϕ is [porosity](#), T is temperature, κ is the [thermal conductivity](#) of the liquid-saturated clast, and x is position. The temperature distribution within the liquid-saturated part of the clast that determines the left-hand side of equation (A.1) depends on u , and we use the solution for steady-state advective-diffusion problem from [Bredehoeft and Papadopoulos \(1965\)](#)

$$(A.2) T(x) - T_a = T_s - T_a e^{\beta x/a} - 1$$

where $\beta = ua/D$ is a dimensionless Peclet number (ratio of advection to diffusion of heat), where D is the [thermal diffusivity](#) of the liquid-saturated clast, a is the distance from the clast surface to the steam–liquid interface, and T_a and T_s are the temperatures of the ambient water and steam–liquid interface, respectively. The solution for the infiltration speed can be obtained by solving equations (A.1) and (A.2)

$$(A.3) u = D \ln[1 + \kappa(T_s - T_a) \rho_s \phi L D]$$

If permeability limits the infiltration speed of water, a lower bound on the velocity is given by [Darcy's law](#) assuming buoyancy controls infiltration

$$(A.4) u > k \rho_w g \mu_w \phi$$

where k is permeability, and μ_w is the viscosity of water. We use $>$ because we neglect the additional (and likely much larger) [pressure gradients](#) from gas contraction and capillary forces that would further increase u .

Whether heat loss controls infiltration (equation (A.3)) or permeable [flow](#) (equation (A.4)) depends on which is larger – the slowest velocity is rate-limiting.

Permeability is not limiting if

$$(A.5) k > \mu_w \phi D \rho_w g \ln[1 + \kappa(T_s - T_a) \rho_s \phi L D]$$

Using $D = D_w \phi + D_r(1 - \phi) = 2.5 \times 10^{-7} \text{ m}^2/\text{s}$ for $\phi = 0.8$, where D_w and D_r are the [diffusivities](#) of water and glass, respectively ([Bagdassarov and Dingwell, 1994](#)), $\kappa = 2 \text{ W m}^{-1} \text{ K}^{-1}$, and conditions at the [ocean surface](#) ($T_s - T_a = 100 \text{ }^\circ\text{C}$, $\rho_s = 1 \text{ kg/m}^3$), we find that cooling is limiting provided $k > 1.2 \times 10^{-13} \text{ m}^2$ for a clast with $a = 1 \text{ m}$. Permeability of pumice is

generally larger than this value, typically $>10^{-12}$ m² for vesicularities of 70–80% (e.g., [Rust and Cashman, 2004](#), [Mueller et al., 2005](#), [Burgisser et al., 2017](#), [Colombier et al., 2017](#); [Gonnermann et al., 2017](#)). Note that the value of k from equation (A.5) is an upper bound because we ignore additional pressure gradients driving water into the clast in equation (A.4) and densities and temperature difference at greater depths decrease the velocity predicted by equation (A.2). The model also neglects any interfacial instabilities that might enhance infiltration or change effective diffusivities (e.g., [Randolph-Flagg et al., 2017](#)).

Appendix B. Cooling, ingestion and ascent model

We model the density evolution and rise of hot and initially water vapor-saturated [clasts](#). Clast density evolves due to internal gas [decompression](#), contraction of vapor by cooling and condensation, and from liquid water infiltration. We assume that the clast vesicularity does not change due to volatile [exsolution](#) after clasts form. By coupling a model for clast density evolution to a model for clast rise speed (equation (3)), we can estimate the time it takes clasts of varying sizes and vesicularities to reach the [ocean surface](#) from a depth of 900 m ([Fig. 6](#)).

Consider a clast that is entirely filled with water vapor such that $f=1$, where f is the fraction of [pore space](#) filled with water vapor. The clast has vesicularity, ϕ , initial temperature, T , diameter, $2R$, and originates from a depth of 900 m. We assume an initial temperature of 850 °C and calculate the initial density ρ_s , mass, m_s , specific [enthalpy](#), H , and total enthalpy, H_T , of internal the water vapor using a [thermodynamic](#) look-up table (IAPWS IF-97, XSteam; [Holmgren, 2006](#)). We assume that the internal steam is fully coupled to the clast and cannot flow out unless the volume of steam exceeds the internal volume of the clast pore space. We calculate clast density as

$$(B.1) \rho_c = \rho_r(1-\phi) + \rho_s\phi + \rho_w\phi(1-f)$$

where the subscripts r and w stand for rock and liquid water. Clast density changes primarily as a function of the volume of internal water vapor, which in turn is affected by cooling and decompression. Clasts lose [thermal energy](#) through cooling according to

$$(B.2) dH_T/dt = -qFS,$$

where q is an average rate of heat loss that was measured experimentally to be approximately 7.5 W cm⁻² for initially air-filled [pumice](#) in water ([Fauria, 2017](#)), S is clast surface area, and F is a factor that describes the partitioning of [latent heat](#) within the water vapor and sensible heat within the glass. The ratio of sensible to latent heat in the clasts is characterized by the Stefan number

$$(B.3) St = \Delta T c_p \phi L \sim 1,$$

where ΔT , is the temperature difference between the initial clast temperature and ambient water, c_p is the [heat capacity](#) of the glass, and L is the latent heat of vaporization. We define

$$(B.4) F = \phi L \Delta T c_p + \phi L.$$

The factor F accounts for sensible heat loss from the glass. That is, not all heat is drawn out of the internal water vapor, rather a proportion of cooling affects the glass. For an 850 °C clast, we estimate $F \sim 0.5$. We find that precise value for F does not affect the calculated clast rise speeds, but is important for determining the minimum clast size that can reach the surface.

We calculate clast rise speeds as a function of clast density and size using equation (3). Clast rise distance Z through the water volume is

$$(B.5) Z = \int U dt.$$

We relate depth h to pressure according to $P = \rho_w g h$. At each new depth we calculate the density and volume, V_s , of the internal water vapor as a function of pressure and specific enthalpy using a thermodynamic lookup table (XSteam; [Holmgren, 2006](#)).

Internal water vapor can expand as clasts rise through the water column, and contract due to cooling. The [volume fraction](#) of pore space filled with water vapor is

$$(B.6) f = V_s \phi V_c$$

where V_c is clast volume. If the net effects of cooling, decompression, and [gas expansion](#) cause the volume of internal water vapor exceed the volume of the pore space such that $f > 1$, we let all excess water vapor exit the pore space and set $f = 1$. We define the excess water vapor as $E_x = f - 1$. We write the change in water vapor mass and total enthalpy due to vapor escape from the clast as

$$(B.7) \Delta m_i = -E_x V_c \phi \rho_s,$$

$$(B.8) \Delta H_T = -\Delta m_i H.$$

In contrast, cooling can make contraction and condensation exceed decompression effects such that $f < 1$. If this is the case, we allow liquid water to enter the pore space vacated due to condensation (e.g., [Fauria et al., 2017](#)). Water ingestion does not decrease clast enthalpy. Equation (B.1) demonstrates, however, how ingested water increases clast density and thereby affects rise speed, decompression rates, and clast fate.

We solve equations (3) and (B.1)–(B.8) using a first order finite difference scheme. The model ends when a clast either reaches the ocean surface or becomes neutrally buoyant due to vapor condensation and water ingestion. [Fig. 4](#) shows how clast size affects rise time to the surface and the minimum clast sizes required to reach the

surface from a depth of 900 m. Below these minimum clast sizes, cooling results in vapor condensation and buoyancy reversal before a clast can reach the surface (Fig. 4). Many of the assumptions in equations (B.2)–(B.8) and approximations needed to develop this model could, in principle, be relaxed with a full 3D [multiphase flow](#) model that includes gas exsolution from the melt and mass, momentum and [energy exchange](#) with the surrounding water, and the presence of unconnected [porosity](#) (Fig. 4). The model used here also neglects the buoyant ascent of warm water that would entrain clasts. A model that couples clast-scale processes and large-scale dynamics may improve the accuracy of calculations of the fate of clasts and may reveal new and neglected processes.

If there is unconnected porosity, and all the connected porosity fills with liquid water, the unconnected porosity is able to keep clasts floating if

$$(B.9)\phi_u=(\rho_r-\rho_w)(\rho_w-\rho_s)(1-\phi_t)$$

where the subscripts on density are as before and u and t indicate unconnected and total porosity, respectively.

Appendix C. Supplementary material

The following is the Supplementary material related to this article.

[Download Acrobat PDF file \(104KB\)](#)[Help with pdf files](#)

Supplement 1. S1 Conduit model parameters.

[Download Acrobat PDF file \(123KB\)](#)[Help with pdf files](#)

Supplement 2. S2 Initial water content.

[Download Acrobat PDF file \(70KB\)](#)[Help with pdf files](#)

Supplement 3. S3 Melt composition.

[Download Acrobat PDF file \(42KB\)](#)[Help with pdf files](#)

Supplement 4. S4 X-ray computed microtomography.

[Download Acrobat PDF file \(180KB\)](#)[Help with pdf files](#)

Supplement 5. S5: [Pumice](#) floatation experiments.

References

[Allen and McPhie, 2009](#)

S.R. Allen, J. McPhie **Products of neptunian eruptions**

Geology, 37 (7) (2009), pp. 639-642

[CrossRefView Record in Scopus](#)

[Allen et al., 2008](#)

S.R. Allen, R.S. Fiske, K.V. Cashman **Quenching of steam-charged pumice: implications for submarine pyroclastic volcanism**

Earth Planet. Sci. Lett., 274 (1) (2008), pp. 40-49

[ArticleDownload PDFView Record in Scopus](#)

[Allen et al., 2010](#)

S.R. Allen, R.S. Fiske, Y. Tamura **Effects of water depth on pumice formation in submarine domes at Sumisu, Izu–Bonin arc, western Pacific**

Geology, 38 (5) (2010), pp. 391-394

[CrossRefView Record in Scopus](#)

[Bagdassarov and Dingwell, 1994](#)

N. Bagdassarov, D. Dingwell **Thermal properties of vesicular rhyolite**

J. Volcanol. Geotherm. Res., 60 (2) (1994), pp. 179-191

[ArticleDownload PDFView Record in Scopus](#)

[Barker et al., 2012](#)

S.J. Barker, M.D. Rotella, C.J. Wilson, I.C. Wright, R.J. Wysoczanski **Contrasting pyroclast density spectra from subaerial and submarine silicic eruptions in the Kermadec arc: implications for eruption processes and dredge sampling**

Bull. Volcanol., 74 (6) (2012), pp. 1425-1443

[CrossRefView Record in Scopus](#)

[Batchelor, 1967](#)

G.K. Batchelor **An Introduction to Fluid Mechanics**

Cambridge University Press, New York (1967)

615 pp

[Bredehoeft and Papaopulos, 1965](#)

J.D. Bredehoeft, I.S. Papaopulos **Rates of vertical groundwater movement estimated from the Earth's thermal profile**

Water Resour. Res., 1 (2) (1965), pp. 325-328

[CrossRefView Record in Scopus](#)

[Burgisser et al., 2017](#)

A. Burgisser, L. Chevalier, J.E. Gardner, J.M. Castro **The percolation threshold and permeability evolution of ascending magmas**

Earth Planet. Sci. Lett., 470 (2017), pp. 37-47

[ArticleDownload PDFView Record in Scopus](#)

[Carey et al., 2014](#)

R.J. Carey, R. Wysoczanski, R. Wunderman, M. Jutzeler **Discovery of the largest historic silicic submarine eruption**

Eos, Trans. Am. Geophys. Union, 95 (19) (2014), pp. 157-159

[CrossRefView Record in Scopus](#)

[Carey et al., 2018](#)

R. Carey, S.A. Soule, M. Manga, J. White, J. McPhie, R. Wysoczanski, F. Caratori-Tontini **The largest deep-ocean silicic volcanic eruption of the past century**

Sci. Adv., 4 (1) (2018), Article e1701121

[CrossRef](#)

[Cas and Giordano,
2014](#)

R.A. Cas, G. Giordano **Submarine volcanism: a review of the constraints, processes and products, and relevance to the Cabo de Gata volcanic succession**

Ital. J. Geosci., 133 (3) (2014), pp. 362-377

[CrossRefView Record in Scopus](#)

[Cas and Wright,
1987](#)

R.A.F. Cas, J.V. Wright **Volcanic Successions, Modern and Ancient: A Geological Approach to Processes, Products and Successions**

(1987)

528 pp

[Cashm
an and
Fiske,
1991](#)

K.V. Cashman, R.S. Fiske **Fallout of pyroclastic debris from submarine volcanic eruptions**

Science (Washington), 253 (5017) (1991), pp. 275-280

[View Record in Scopus](#)

[C
o
l
o
m
b
i
e
r
-
e
t
-
a
l
-
-
-](#)

[2](#)
[0](#)
[1](#)
[7](#)

M. Colombier, F.B. Wadsworth, L. Gurioli, B. Scheu, U. Kueppers, A. Di Muro, D.B. Dingwell **The evolution of pore connectivity in volcanic rocks**

Earth Planet. Sci. Lett., 462 (2017), pp. 99-109

[ArticleDownload PDFView Record in Scopus](#)

[Costa, 2005](#)

A. Costa **Viscosity of high crystal content melts: dependence on solid fraction**

Geophys. Res. Lett., 32 (22) (2005), [10.1029/2005GL024303](#)

[Degruyter et al., 2012](#)

W. Degruyter, O. Bachmann, A. Burgisser, M. Manga **The effects of outgassing on the transition between effusive and explosive silicic eruptions**

Earth Planet. Sci. Lett., 349 (2012), pp. 161-170

[ArticleDownload PDFView Record in Scopus](#)

[Dufek et al., 2007](#)

J. Dufek, M. Manga, M. Staedter **Littoral blasts: pumice–water heat transfer and the conditions for steam explosions when pyroclastic flows enter the ocean**

J. Geophys. Res., Solid Earth, 112 (B11) (2007), [10.1029/2006JB004910](#)

[Fauria, 2017](#)

K. Fauria

PhD Dissertation

University of California, Berkeley (2017)

[Fauria et al., 2017](#)

K.E. Fauria, M. Manga, Z. Wei **Trapped bubbles keep pumice afloat and gas diffusion makes pumice sink**

Earth Planet. Sci. Lett., 460 (2017), pp. 50-59

[ArticleDownload PDFView Record in Scopus](#)

[Giachetti et al., 2010](#)

T. Giachetti, T.H. Druitt, A. Burgisser, L. Arbaret, C. Galven **Bubble nucleation, growth and coalescence during the 1997 vulcanian explosions of Soufrière Hills Volcano, Montserrat**

J. Volcanol. Geotherm. Res., 193 (3) (2010), pp. 215-231

[ArticleDownload PDFView Record in Scopus](#)

[Giordano et al., 2010](#)

D. Giordano, J.K. Russell, D.B. Dingwell **Viscosity of magmatic liquids: a model**

Earth Planet. Sci. Lett., 271 (1) (2008), pp. 123-134

[ArticleDownload](#) [PDFView](#) [Record in Scopus](#)

[Gonnermann and](#)

H.M. Gonnermann, M. Manga **Nonequilibrium magma degassing: results from modeling of the ca. 1340 AD eruption of Mono Craters, California**

Earth Planet. Sci. Lett., 238 (1) (2005), pp. 1-16

[ArticleDownload](#) [PDFView](#) [Record in Scopus](#)

[Gonnermann et al.](#)

H. Gonnermann, T. Giachetti, C.T. Nguyen, B.F. Houghton, J.A. Crozier, R.J. Carey **Permeability during magma expansion and compaction**

J. Geophys. Res., Solid Earth (2017)

[Holmgren, 2006](#)

M. Holmgren **X steam for Matlab**

www.x-eng.com (2006), Accessed 20th Nov 2017

[Houghton et al.](#)

B.F. Houghton, B.J. Hobden, K.V. Cashman, C.J.N. Wilson, R.T. Smith **Large-scale interaction of lake water and rhyolitic magma during the 1.8 Ka Taupo Eruption, New Zealand**

Explosive Subaqueous Volcanism (2003), pp. 97-109

[CrossRefView](#) [Record in Scopus](#)

[Jutzeler et al., 20](#)

M. Jutzeler, R. Marsh, R.J. Carey, J.D. White, P.J. Talling, L. Karlstrom **On the fate of pumice rafts formed during the 2012 Havre submarine eruption**

Nat. Commun., 5 (2014), [10.1038/ncomms4660](https://doi.org/10.1038/ncomms4660)

[Jutzeler et al., 20](#)

M. Jutzeler, M. Manga, J.D.L. White, P.J. Talling, A.A. Proussevitch, S.F.L. Watt, R.N. Cassidy, A. Le Friant, O. Ishizuka **Submarine deposits from pumiceous pyroclastic density currents traveling over water: an outstanding example from offshore Montserrat (IODP 340)**

Bull. Geol. Soc. Am., 129 (3–4) (2017), pp. 392-414

[CrossRefView](#) [Record in Scopus](#)

[Kano, 2003](#)

K. Kano **Subaqueous pumice eruptions and their products: a review**

Explosive Subaqueous Volcanism (2003), pp. 213-229

[CrossRefView](#) [Record in Scopus](#)

[Kano et al., 1996](#)

K. Kano, T. Yamamoto, K. Ono **Subaqueous eruption and emplacement of the Shinjima Pumice, Shinjima (Moeshima) Island, Kagoshima Bay, SW Japan**

J. Volcanol. Geotherm. Res., 71 (2–4) (1996), pp. 187-206

[ArticleDownload](#) [PDFView](#) [Record in Scopus](#)

[Kato Y, 1987](#)

Y. Kato **Woody pumice generated with submarine eruption**

J. Geol. Soc. Jpn., 93 (1987), pp. 11-20

[View Record in Scopus](#)

[Kozono and Koy](#)

T. Kozono, T. Koyaguchi **Effects of relative motion between gas and liquid on 1-dimensional steady flow in silicic volcanic conduits, 2: origin of diversity of eruption styles**

J. Volcanol. Geotherm. Res., 180 (1) (2009), pp. 37-49

[ArticleDownload PDFView Record in Scopus](#)

[Kueppers et al.,](#)

U. Kueppers, A.R.L. Nichols, V. Zanon, M. Potuzak, J.M.R. Pacheco **Lava balloons – peculiar products of basaltic submarine eruptions**

Bull. Volcanol., 74 (2012), pp. 1379-1393

[CrossRefView Record in Scopus](#)

[Llewellyn and Ma](#)

E.W. Llewellyn, M. Manga **Bubble suspension rheology and implications for conduit flow**

J. Volcanol. Geotherm. Res., 143 (1) (2005), pp. 205-217

[ArticleDownload PDFView Record in Scopus](#)

[Manville et al., 1](#)

V. Manville, J.D.L. White, B.F. Houghton, C.J.N. Wilson **The saturation behaviour of pumice and some sedimentological implications**

Sediment. Geol., 119 (1) (1998), pp. 5-16

[ArticleDownload PDFView Record in Scopus](#)

[McPhie and Allen](#)

J. McPhie, R.L. Allen **Submarine, silicic, syn-eruptive pyroclastic units in the Mount Read Volcanics, Western Tasmania: influence of vent setting and proximity on lithofacies characteristics**

Explosive Subaqueous Volcanism (2003), pp. 245-258

[CrossRefView Record in Scopus](#)

[Mueller et al., 20](#)

S. Mueller, O. Melnik, O. Spieler, B. Scheu, D.B. Dingwell **Permeability and degassing of dome lavas undergoing rapid decompression: an experimental determination**

Bull. Volcanol., 67 (6) (2005), pp. 526-538

[CrossRefView Record in Scopus](#)

[National Academ](#)

National Academies of Sciences, Engineering and Medicine **Volcanic Eruptions and Their Repose, Unrest, Precursors, and Time**

The National Academies Press, Washington, DC (2017), [10.17226/24650](#)

[Olson and Singe](#)

P. Olson, H. Singer **Creeping plumes**
J. Fluid Mech., 158 (1985), pp. 511-531
[CrossRefView Record in Scopus](#)

[Papale, 1999](#)

P. Papale **Strain-induced magma fragmentation in explosive eruptions**
Nature, 397 (6718) (1999), pp. 425-428
[CrossRefView Record in Scopus](#)

[Putirka, 2008](#)

K.D. Putirka **Thermometers and barometers for volcanic systems**
Rev. Mineral. Geochem., 69 (1) (2008), pp. 61-120
[CrossRefView Record in Scopus](#)

[Randolph-Flagg](#)

N. Randolph-Flagg, S. Breen, A. Hernandez, M. Manga, S. Self **Evenly spaced columns in the Bishop Tuff (California, USA) as relicts of hydrothermal cooling**
Geology, 45 (11) (2017), pp. 1015-1018
[CrossRefView Record in Scopus](#)

[Reynolds et al., 1980](#)

M.A. Reynolds, J.G. Best, R.W. Johnson **1953–57 Eruption of Tulumán Volcano: Rhyolitic Volcanic Activity in the Northern Bismarck Sea, vol. 7**
Geological Survey of Papua New Guinea (1980)

[Risso et al., 2002](#)

C. Risso, R.A. Scasso, A. Aparicio **Presence of large pumice blocks on Tierra del Fuego and South Shetland Islands shorelines, from 1962 South Sandwich Islands eruption**
Mar. Geol., 186 (3) (2002), pp. 413-422
[ArticleDownload PDFView Record in Scopus](#)

[Rotella et al., 2013](#)

M.D. Rotella, C.J. Wilson, S.J. Barker, I.C. Wright **Highly vesicular pumice generated by buoyant detachment of magma in subaqueous volcanism**
Nat. Geosci., 6 (2) (2013), p. 129, [10.1038/ngeo1709](#)
[CrossRefView Record in Scopus](#)

[Rotella et al., 2015](#)

M.D. Rotella, C.J. Wilson, S.J. Barker, C.I. Schipper, I.C. Wright, R.J. Wysoczanski **Dynamics of deep submarine silicic explosive eruptions in the Kermadec arc, as reflected in pumice vesicularity textures**
J. Volcanol. Geotherm. Res., 301 (2015), pp. 314-332
[ArticleDownload PDFView Record in Scopus](#)

[Rust and Cashman](#)

A.C. Rust, K.V. Cashman **Permeability of vesicular silicic magma: inertial and hysteresis effects**

Earth Planet. Sci. Lett., 228 (1) (2004), pp. 93-107

[ArticleDownload](#) [PDFView](#) [Record in Scopus](#)

[Shea et al., 2013](#)

T. Shea, J. Hammer, E. First **Magma balloons or bombs?**

Nat. Geosci., 6 (10) (2013), pp. 802-803

[CrossRefView](#) [Record in Scopus](#)

[Simmons, 1998](#)

J.H. Simmons **What is so exciting about non-linear viscous flow in glass, molecular dynamics simulations of brittle fracture and semiconductor–glass quantum composites**

J. Non-Cryst. Solids, 239 (1) (1998), pp. 1-15

[ArticleDownload](#) [PDFView](#) [Record in Scopus](#)

[Vella and Huppert, 2007](#)

D. Vella, H.E. Huppert **The waterlogging of floating objects**

J. Fluid Mech., 585 (2007), pp. 245-254

[CrossRefView](#) [Record in Scopus](#)

[van Otterloo et al., 2015](#)

J. van Otterloo, R.A. Cas, C.R. Scutter **The fracture behaviour of volcanic glass and relevance to quench fragmentation during formation of hyaloclastite and phreatomagmatism**

Earth-Sci. Rev., 151 (2015), pp. 79-116

[ArticleDownload](#) [PDFView](#) [Record in Scopus](#)

[von Lichten et al., 2016](#)

I.J. von Lichten, J.D.L. White, V. Manville, C. Ohneiser **Giant rafted pumice blocks from the most recent eruption of Taupo volcano, New Zealand: insights from palaeomagnetic and textural data**

J. Volcanol. Geotherm. Res., 318 (2016), pp. 73-88

[ArticleDownload](#) [PDFView](#) [Record in Scopus](#)

[White et al., 2015](#)

J.D. White, C.I. Schipper, K. Kano **Submarine explosive eruptions**

The Encyclopedia of Volcanoes (second edition) (2015), pp. 553-569

[ArticleDownload](#) [PDFView](#) [Record in Scopus](#)

[Whitham and Sparks, 1986](#)

A.G. Whitham, R.S.J. Sparks **Pumice**

Bull. Volcanol., 48 (4) (1986), pp. 209-223

[CrossRefView](#) [Record in Scopus](#)

[Wilson and Walker, 1985](#)

C.J.N. Wilson, G.P. Walker **The Taupo eruption, New Zealand, I: general aspects**

Philos. Trans. R. Soc. Lond. A, Math. Phys. Eng. Sci., 314 (1529) (1985), pp. 199-228

[CrossRefView](#) [Record in Scopus](#)

[Wright et al., 2006](#)

H. Wright, J.J. Roberts, K.V. Cashman **Permeability of anisotropic tube pumice: model calculations and measurements**

Geophys. Res. Lett., 33 (17) (2006), [10.1029/2006GL027224](https://doi.org/10.1029/2006GL027224)